Hindawi
Advances in Civil Engineering
Volume 2018, Article ID 9818250, 15 pages
https://doi.org/10.1155/2018/9818250

Research Article

Cracking and Failure in Rock Specimen Containing Combined Flaw and Hole under Uniaxial Compression

Xiang Fan,[1,2,3,4] Rui Chen,[1] Hang Lin,[5] Hongpeng Lai,[1] Chunyang Zhang,[6] and Qihua Zhao[2]

[1]*School of Highway, Chang'an University, Xi'an 710064, China*
[2]*State Key Laboratory of Geohazard Prevention and Geoenvironment Protection, Chengdu University of Technology, Chengdu 610059, China*
[3]*Key Laboratory of Bridge Engineering Safety Control by Hunan Province, Department of Education, Changsha University of Science and Technology, Changsha 410114, China*
[4]*Engineering Research Center of Catastrophic Prophylaxis and Treatment of Road and Traffic Safety of Ministry of Education, Changsha University of Science and Technology, Changsha 410004, China*
[5]*School of Resources and Safety Engineering, Central South University, Changsha 410083, China*
[6]*School of Resources and Environment Engineering, Wuhan University of Technology, Wuhan 430070, China*

Correspondence should be addressed to Hang Lin; linhangabc@126.com and Qihua Zhao; zhqh@163.com

Received 20 September 2017; Revised 3 February 2018; Accepted 18 February 2018; Published 2 May 2018

Academic Editor: Cumaraswamy Vipulanandan

Flaw is a key factor influencing failure behavior of a fractured specimen. In the present study, rectangular-flawed specimens were prepared using sandstone to investigate the effect of flaw on failure behavior of rock. Open flaw and cylindrical hole were simultaneously precut within rock specimens using high-pressure water jet cutting technology. Five series of specimens including intact, single-hole-alone, two-hole-alone, single-hole and two-flaw, and two-hole and single-flaw blocks were prepared. Uniaxial compressive tests using a rigid servo control instrument were carried out to investigate the fracture processes of these flawed specimens. It is observed that during loading, internal stress always intensively distributed at both sidewalls of open hole, especially at midpoint of sidewalls, so rock crumb flaking was firstly observed among all sandstone specimens containing single hole or two holes. Cracking around open hole is associated with the flaw inclination angle which was observed in Series III and V. Crack easily initiated at the tips of flaw with inclination angles of 0°, 30°, and 60° but hard for 90° in Series III and V. Rock burst was the major failure mode among most tested specimens, which generally induced new cracks and finally created crater shape. Additionally, due to extrusion between blocks, new shear or tensile cracks were generated and the rock specimen surface spalled. Eventually, four typical failure processes including rock crumb flaking, crack initiation and propagation, rock burst, and second rupture, were summarized.

1. Introduction

It is well known that rock mass is discontinuous and inhomogeneous due to numerous joints, cleavages, beddings, and faults presented within it. The increasing number of engineering practice, such as mining, tunneling, and hydraulic power station, has fueled growing research interests on fractured rock mass. Understanding the mechanical behavior of fractured rock mass is the key to ensure engineering safety and efficiency. Since the mechanical behavior of rock mass is controlled by rock discontinuities, rock engineering practitioners have been attempting to relate rock mechanics to rock joints via theoretical analysis, experimental testing and numerical simulation [1–7]. Among the published reports, experimental investigation was probably the widely used method.

Researchers have used many rock-like materials, such as gypsum, cement, and PMMA (poly methyl meth acrylate), to study the mechanical behavior of fractured rock [8–10]. The advantage of using rock-like materials is that the number

and geometry of flaws, open or closed, could be easily premanufactured, and therefore, the fractured rock properties could be quantitatively analyzed. Research has found that the axial strength of a rock specimen was closely related to flaw length and flaw inclination angle, and a number of relationships reveal that uniaxial compressive strength (UCS) of rock decreases with increasing flaw length. However, no complete consensus is achieved on the relationships between UCS and flaw inclination. In Liu's study [11], specimens with flaws parallel to the loading direction showed minimum UCS, while those with flaws perpendicular to the loading exhibited the maximum. However, another study, reported by Yang and Jing [12], showed that a minimum UCS was obtained when flaw inclines 45° to the loading direction, while a maximum UCS was obtained with flaw inclined 90° to the loading direction. Generally, the maximum UCS is found with flaw inclined 90° to the loading direction, but the minimum UCS was obtained with flaw inclined at various angles. In fact, rock strength is influenced by several factors, such as material type, flaw geometry, sample dimension, and even testing method [13–15].

In the past studies of fracture characteristics of real rock or rock-like materials containing flaws, to better and clearly view crack development, high-speed camera was often used to record cracking process [16]. Flaw configurations affect not only rock strength but also cracking pattern, so many experimental studies were performed to identify crack initiation or coalescence type [17–27]. It has been found that for fractured rock subjected to compressive loading, crack initiates first around flaw tips, and tensile crack was mostly observed. Cracking process was directly related to the failure mode. For decades, many failure modes have been identified and summarized, such as stepped failure, shear failure, cleavage, and so on [14, 28].

In the studies mentioned above, internal defect within the tested specimen was set as two-dimensional open flaw, which cannot represent real status of flaw in natural rock. So researchers have carried out studies to investigate the effect of three-dimensional flaw on rock fracture, which can be referred to Adams and Sines [29], Germanovich et al. [30], and Dyskin et al. [31]. Circular openings scarcely exist within natural rock mass, but excavation may create circular cavities including laneway, tunnel, and culvert. To model stress change and failure behavior around opening created by engineering construction, experimental and numerical approaches were widely used. In experimental studies, cylindrical cavity was usually precut and researchers mainly focused on failure characteristics around openings [32–39]. Zhao et al. [40] used acoustic emission technology to investigate cracking process around open hole. Li et al. [41] found a blast-induced pit of a single-hole sandstone specimen under uniaxial loading and crater volume was related to impact load. Zhao et al. [38] used experimental and numerical methods to study failure characteristics of rock-like materials with an open hole and found that peak strength was related to sample width and hole diameter. In field test, the excavation-damaged zone was adjacent to underground opening, two zones including damaged and disturbed zones were identified, which was considered as a result of redistribution of stresses [42, 43]. Generally, the physical model was mostly employed, but sometimes it is unable to evaluate internal stress distribution according to current techniques, so the numerical method was used to assist physical studies. In the numerical studies of cracking process, a distinct element method, particle flow code, was widely used to simulate crack initiation and propagation of single flaw or multiflaw specimens under uniaxial or biaxial compression loading [7, 44, 45]. Using particle flow code approach, circular opening was created within the intermittently jointed model, and it was found that the dip angle of joint greatly impacts fracture behavior around opening [46, 47]. Using rock failure process analysis approach, horseshoe-shaped opening was created, and the failure process and stress change around opening were obtained [48, 49]. In numerical simulation, internal stress evolution around flaw and opening can be well recorded, and fracture process can be modeled.

Previous studies indicate that joint significantly impacts fracture characteristics of jointed rock containing hole and joint. To further understand the influence of joint on failure behavior of a hole-containing model, a combination of open flaw and circular hole was designed to premanufacture in rectangular rock samples. Experimental and numerical approaches were employed to investigate the failure process of rock specimens containing both flaw and hole under uniaxial compressive loading. The study aims to investigate the interaction between hole and flaw location and the influence of the inclination angle of flaw around hole on cracking process, which contributes to good understanding of influence of flaw location and orientation on damaged zones of circular openings in rock mechanics.

2. Sample Preparation and Testing Method

2.1. Sample Preparation. In the present study, sandstone was chosen to prepare cuboid specimens containing precasted holes and flaws. The specimen dimensions were 100 mm × 100 mm × 30 mm (height × length × width). In the present study, five series of experimental specimens were prepared as listed in Table 1. The cuboid intact blocks named Series I (Figure 1(a)) were firstly prepared. The two sample ends were grinded off to become smooth using two parallel grinding wheels. Afterwards, the intact specimens were further made into fractured specimens. High-pressure water jet cutting technology was used to produce open flaw and/or hole in Series I specimens. As shown in Figure 1(b), the Series II specimen contains one single hole at the specimen center which is coincided with circle center of open hole and origin of the coordinates. Figure 1(c) shows the Series III specimen, which contains a single hole and two flaws locating at both sides of open hole, and the flaw midpoint was fixed on x-axis and 30 mm away from the specimen center. The specimen containing two open holes is named Series IV, as shown in Figure 1(d). The circle centers of the two open holes were fixed on x-axis with spacing 20 mm away from the specimen center. On the basis of Series IV, flawed specimens having two holes and one single flaw were further prepared, named Series V as shown in Figure 1(e). One single flaw is

Table 1: Arrangement of specimens.

Series	Specimen type	α (°)	Sample ID
I	Intact specimen (Figure 1(a))	—	—
II	Single-hole specimen without flaw (Figure 1(b))	—	SHWF
III	Single-hole and two-flaw specimen (Figure 1(c))	0	SHTF-0
		30	SHTF-30
		60	SHTF-60
		90	SHTF-90
IV	Two-hole specimen without flaw (Figure 1(d))	—	THWF
V	Two-hole and single-flaw specimen (Figure 1(e))	0	THSF-0
		30	THSF-30
		60	THSF-60
		90	THSF-90

created between two holes while the flaw midpoint is coincided with the specimen center. Note that radius (r) of all open holes and flaw length (L) are both 10 mm as shown in Figure 1. The thickness of all flaws is about 2 mm. The internal faces of flaws and circular openings are smooth. The flaw inclination angle, α, changed by rotating along its midpoint in anticlockwise direction at an interval of 30° from 0° to 90°, and therefore, there would be four inclination cases for each fractured specimen with one or two flaws. In order to make the discussion clear in the following section, name of each edge of open hole is defined in Figure 1(f).

2.2. Testing Method. For the purpose of viewing failure process and measuring compressive strength, destructive tests of the rock specimen were conducted on a rigid servo control machine. Figure 2 shows the testing system. The loading instrument basement was fixed on the ground, and the upper loading platen with a high stiffness moves along two columns under hydraulic pressure while lower platen remained stationary. Two ends of the specimen were daubed with lubricant to decrease end effect. While loading, axial stress and displacement were recorded by a computer system. The failure process was recorded by a camera located in front of the testing specimen. Testing on the intact specimens shows that average compressive strength is 85.35 MPa, elastic modulus is 34.87 GPa, and Poisson's ratio is 0.2195.

3. Failure Characteristics

3.1. Failure of Single-Hole-Alone and Two-Hole-Alone Specimens. As illustrated in Figure 3(a), no obvious crack initiation was observed in the early loading phase. When axial stress was close to the peak value, crack initiated and rapidly developed across the specimen, and simultaneously, axial stress dropped approximately vertically. Due to openings within the rock specimen (Figures 3(b) and 3(c)), stress concentrates at both sidewalls of the open hole in the SHWF specimen. Rock crumb flaking shown in Figure 3(d) was first observed during loading. At the moment of complete failure, the rock fragment ejected and huge sonic generated, which was called rock burst in this study. The cracks shown in Figure 3(b) were momentarily generated because of instantaneous rock burst. For the THWF specimen, internal stress distribution was different from that of the SHWF specimen under compressive loading. Similarly, stress concentration still occurred at both sides of open hole, but internal stress superposition occurred between two holes, and therefore, the maximum internal stress was located between two holes. So rock crumb flaking was first observed at internal sidewalls of two openings. Identically, rock burst occurred at maximum stress location, that is, the ligament zone between two holes. Rock burst resulted in surface rock ejection and another four cracks as shown in Figure 4(c). For high-strength brittle materials, as axial strain increased, elastic strain energy accumulated at stress concentrated zone. When external loading exceeded intrinsic strength of materials, elastic strain energy suddenly released companying with rock fragment ejection and huge sonic. So the failure process of SHWF and THSF specimens obviously differs from that of the intact one in the condition of uniaxial compression.

3.2. Failure of SHTF Specimens. Flaw geometry is a key factor influencing failure behavior and strength of the fractured specimens. Figure 4 shows the failure process of the SHTF-0 specimen under uniaxial compression. The stress-strain curve is shown to relate failure status with the corresponding axial stress level as shown in Figure 4(a). Obviously, when the flaw inclination angle was 0°, flaw and hole dramatically reduced the net section area bearing compressive stress, and the minimum section area across hole center was 60% of overall horizontal section area. During loading, the SHTF-0 specimen also experienced internal stress concentration. When axial stress approached 60% of peak axial stress, rock crumb flaked off from sidewall and fell to bottom of cylindrical hole as seen from Figure 4(b). The two zero-degree flaws were located within the stress concentration zone, and hence, internal stress around open hole was redisturbed. When the axial stress level was more than 70% of peak strength, cracks started initiating. Crack initiation at flaw tips shown in Figure 4(c) indicates that stress redistribution occurs around open flaw. Actually, tensile stress concentrated at flaw tip, so tensile cracks were generated. Also, another tensile crack occurred at right flaw tip. At the moment of peak strength, the ligament zones connecting flaw tip and hole side edge were crushed, but no

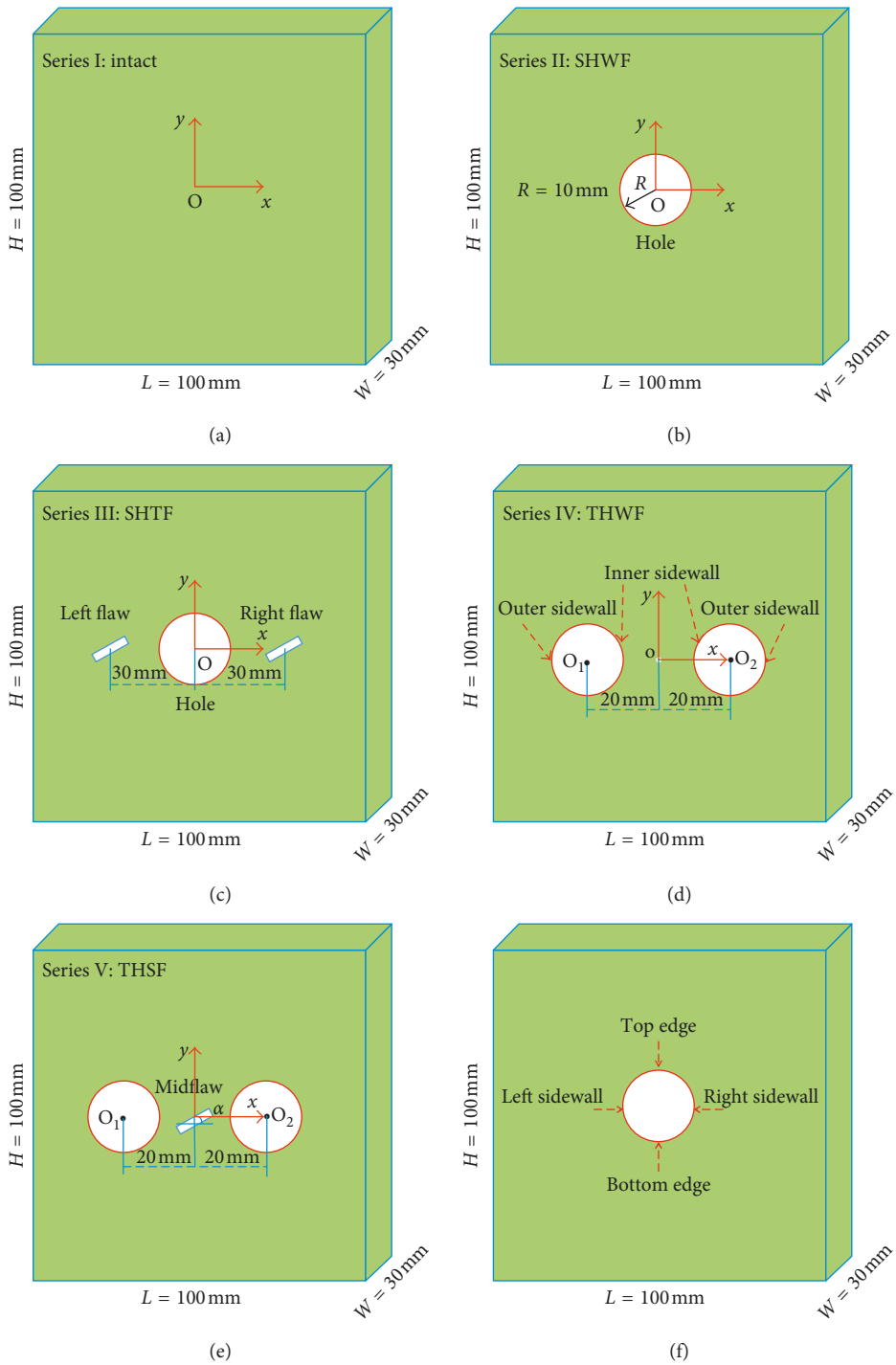

Figure 1: Schematic diagrams of fractured rock specimens: (a) Series I; (b) Series II; (c) Series III; (d) Series IV; (e) Series V; (f) illustration of hole edges.

instantaneous burst occurred. Due to extrusion between upper and lower blocks after peak stress, surface rock spalled at the ligament zone (Figure 4(d)).

Figure 5 shows the failure process of the SHTF-30 specimen under uniaxial compression. Similarly, when the axial stress level was about 60% of peak strength, rock crumb flaking at sidewalls was first observed (Figures 5(a) and 5(b)). And then, like SHTF-0 specimen, tensile cracks initiated at flaw tips as shown in Figure 5(c) and then propagated towards top and bottom ends of the specimen. It also indicates that for 30° inclination angle, internal stress still would concentrate at flaw tip and further creates cracks. Continuous loading brought about increase in axial strain and elastic strain energy accumulation. At the moment of elastic strain energy releasing with huge sonic as illustrated in Figure 5(d), rock fragments ejected out. Parts of fragments

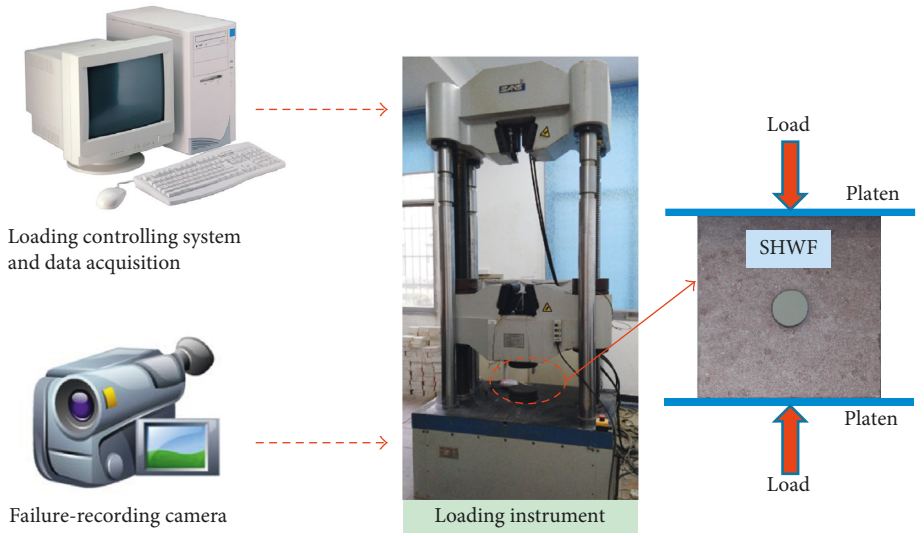

Figure 2: Schematic of loading and recording systems.

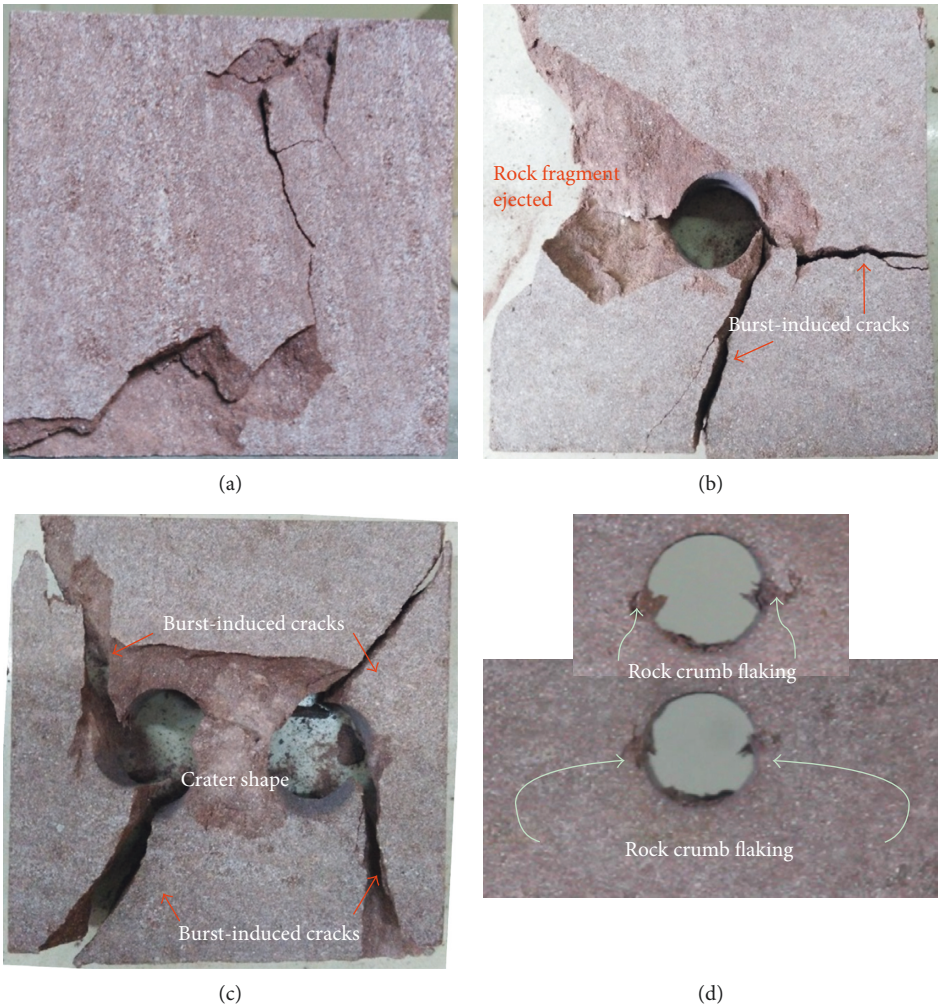

Figure 3: Photographs of final failure for (a) intact specimen, (b) specimen containing single hole only, (c) specimen containing two holes only, and (d) rock crumb flaking.

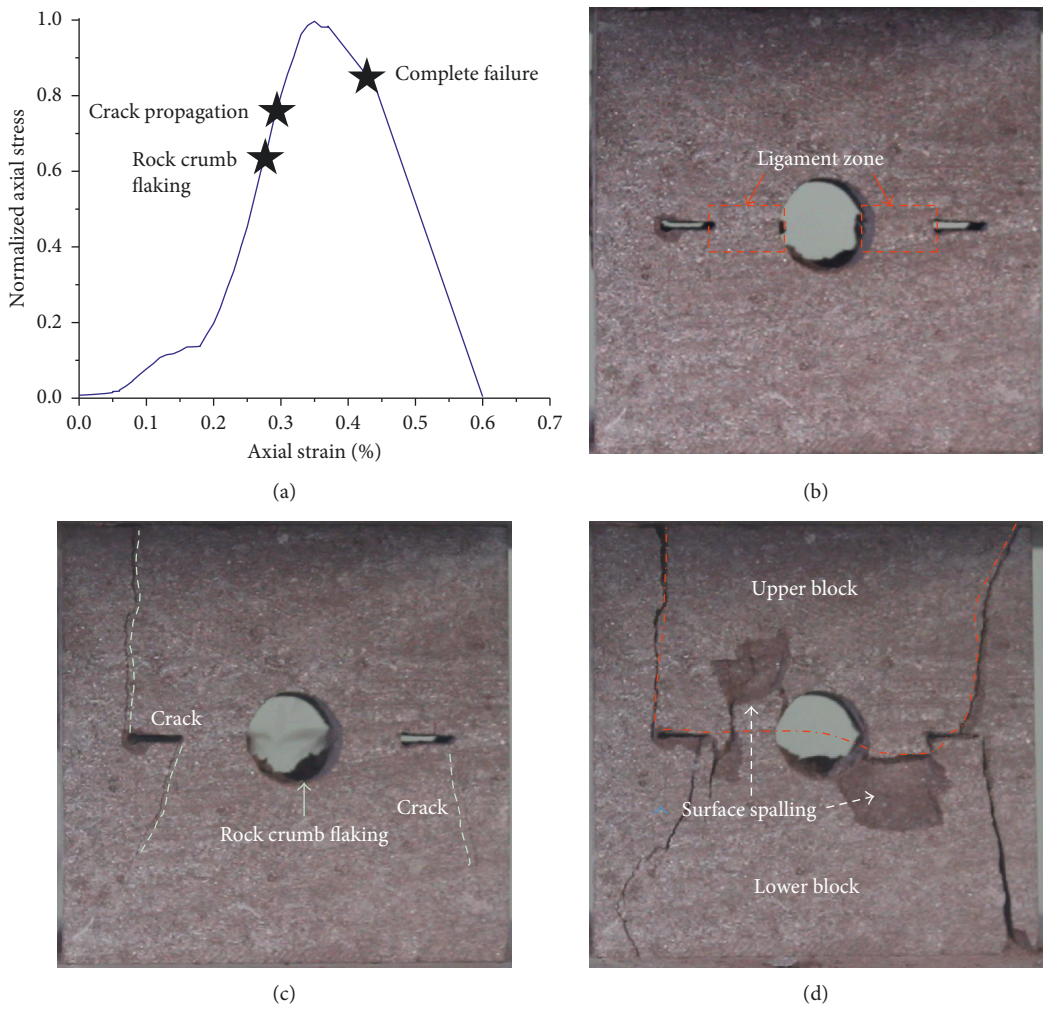

Figure 4: Failure process of the SHTF-0 specimen: (a) stress-strain curve of SHTF-0; (b) rock crumb flaking; (c) crack propagation; (d) complete failure.

were crushed into sand grain and flied out. The phenomenon was also regarded as rock burst. At that moment, axial stress reached peak and then sharply dropped. Some fragments flied away several meters. Occurrence of rock burst meant that the specimen completely failed. In addition, intensive rock burst also generated cracks which was called burst-induced crack in the present study. In Figure 5(e), cracks around right flaw were induced by rock burst.

Figure 6 shows the failure process of the SHTF-60 specimen under uniaxial compression. For the SHTF-60 specimen, combing the stress-strain curve (Figure 6(a), when the axial stress level was more than 60% of peak one, at first failure phase, rock crumb flaking still occurred at midpoint of hole side edge (Figure 6(b)). It was obviously observed that surface crack initiated at side edge and propagated towards adjacent flaw tip, but the crack merely developed on surface at the stress level of 80% of peak strength (Figure 6(c)), which then lead surface rock ejecting towards free face. And finally two craters were generated between hole and flaws at peak stress. After generation of crater shape, due to unequal fall of block above hole, a shear crack formed at the upper right corner as shown in Figure 6(d). For the time being, the ligament zone between hole and flaws did not run through the thickness and still can bear loading. As loading continued after peak stress, more intense surface spalling was observed, which caused surface rock eject again. This failure was called second rupture shown in Figure 6(e). Second rupture occurred because stress concentrated at the ligament zone again.

Figure 7 shows the failure process of the SHTF-90 specimen under uniaxial compression. For the SHTF-90 specimen, the early failure phase was analogous to that of the other SHTF specimens. In the early failure phase of SHTF specimens at the stress level of 60% of peak stress (Figure 7(a)), rock crumb flaking first occurred at internal stress-concentrated locations as shown in Figure 7(b), but finally no crack created around open hole until occurrence of rock burst (Figure 7(c)). Also, rock burst directly resulted in the sharp decrease in axial stress. Rock burst caused surface rock around circular openings to spall and generated several burst-induced cracks as shown in Figure 7(d). From the overall failure of the SHTF-90 specimen, 90° flaws scarcely affected the failure mode.

In the process of compressive loading, failure occurring at hole sidewalls may be observed on front face or opposite

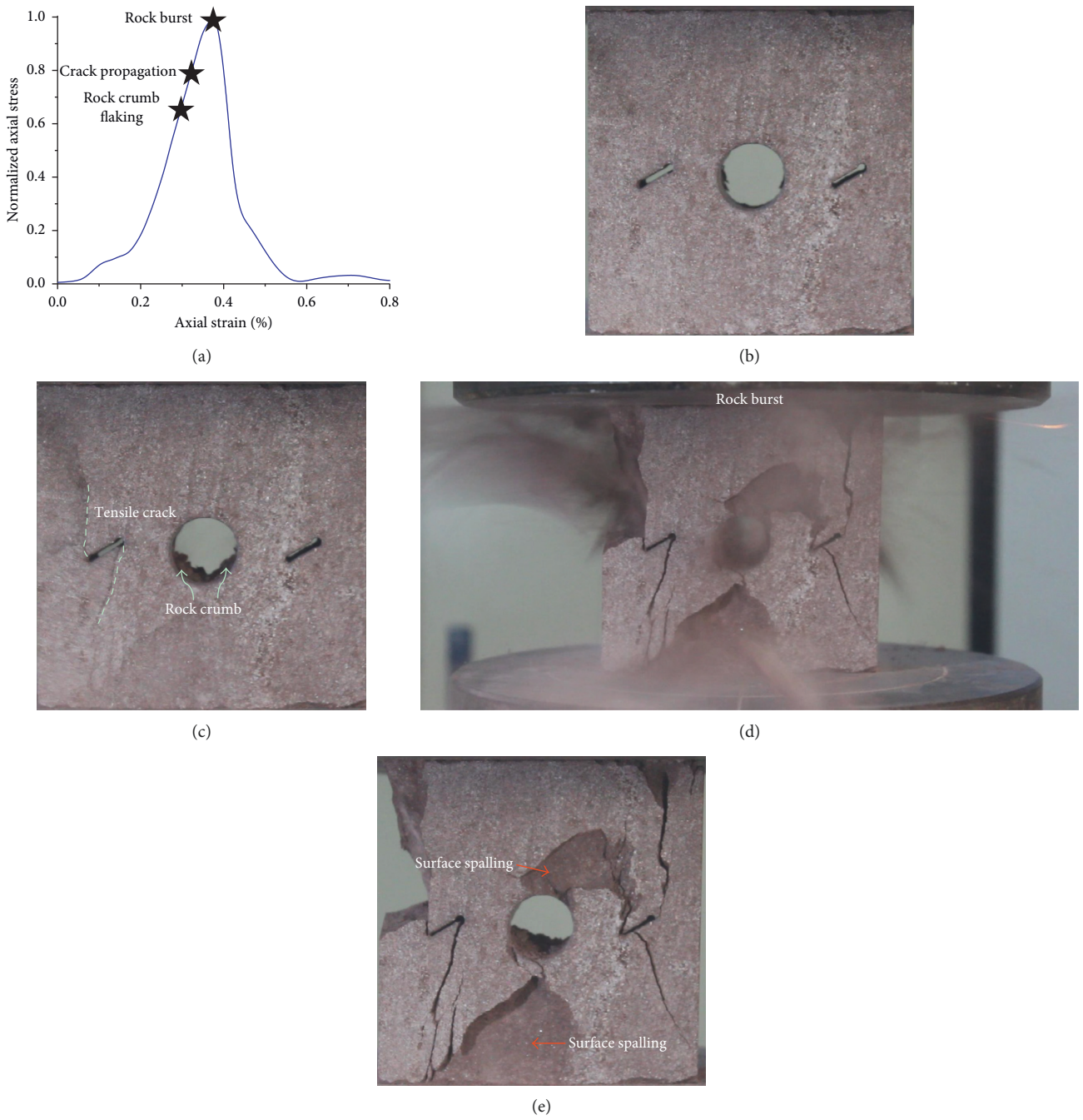

Figure 5: Failure process of the SHTF-30 specimen: (a) stress-strain curve of SHTF-30; (b) rock crumb flaking; (c) crack propagation; (d) rock burst: (e) complete failure.

face. When $\alpha = 0^{\circ}$, tensile crack initiated at flaw tips. It is well known that tensile strength of rock is much lower of its compressive strength. The generated tensile crack extended along loading direction. In fact, it is quite short from observable crack initiation to specimen complete failure, so high-velocity camera was usually used to record failure process. When $\alpha = 30^{\circ}$, the failure process is similar to that of the SHTF specimen with $\alpha = 30^{\circ}$. By comparing four different inclined cases of SHTF specimens, it can be found that crack easily initiated at tips of 0° and 30° flaws. Surface cracking process was observed for the SHTF-60 specimen; surface spalling was easily observed for SHTF-60 and -90 specimens; and crater shape was created after rock burst.

3.3. Failure of Fractured Specimen with Two Holes. According to failure of the THWF specimen, it is known that the internal stress concentration zone is located between two holes, which leads to surface rock spalling. Compared with the THWF specimen in uniaxial compression, existence of midflaw would further disturb stress distribution between two holes. The inclination angle of midflaw changed from

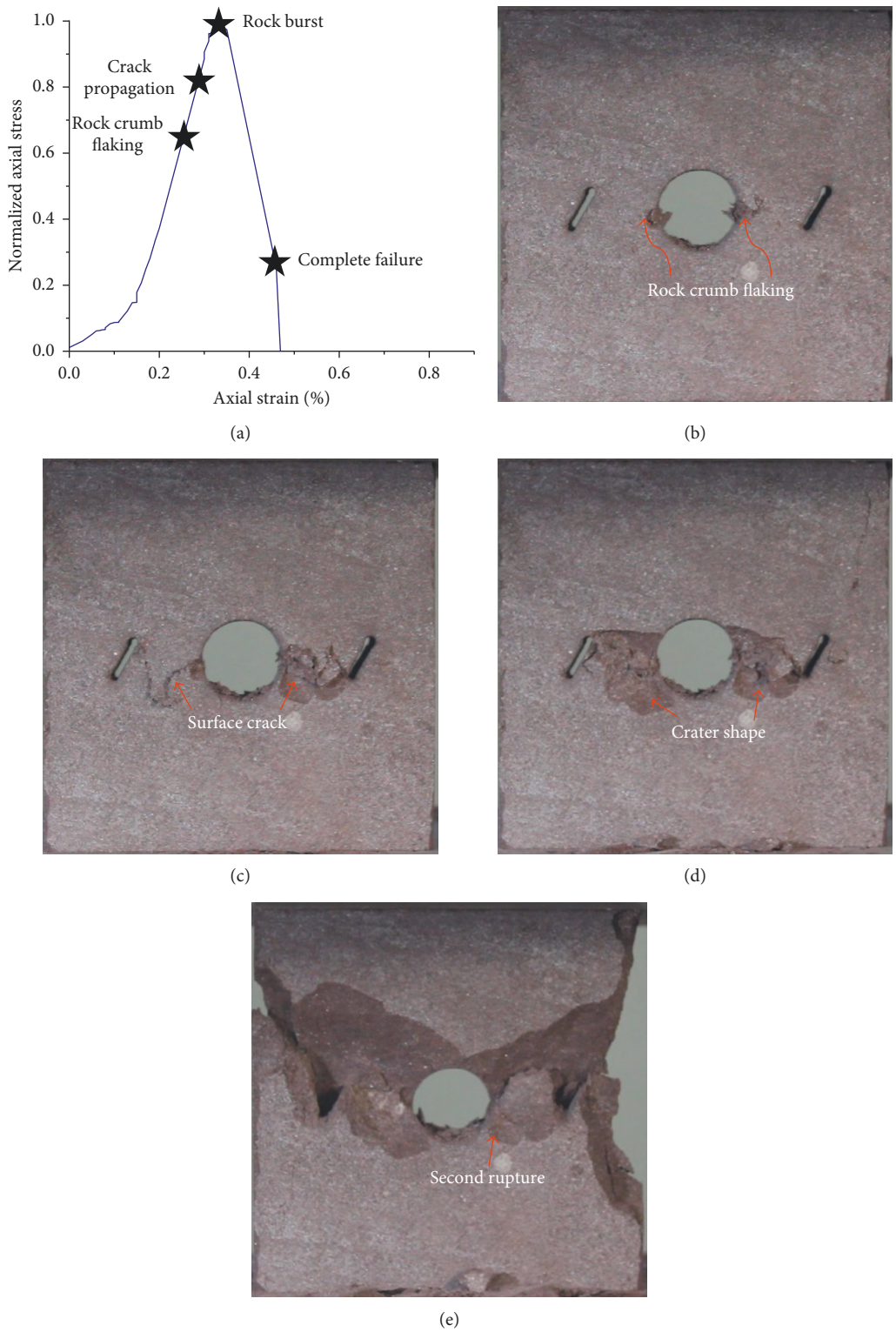

Figure 6: Failure process of the SHTF-60 specimen: (a) stress-strain curve of SHTF-60; (b) rock crumb flaking; (c) surface crack propagation; (d) burst-induced crater; (e) complete failure.

0° to 90°, which results in a substantial reduction in section area across circle centers. The net section area was 50% of the specimen section area for 0° flaw and 60% for 90° flaw. The distance between flaw tip and adjacent hole edge ranges from 5 mm for 0° flaw to 9 mm for 90° flaw. Failure process of THSF-30 was basically similar to that of THSF-60, so only one failure case of THSF-60 was shown. For THSF specimens, in the loading process, rock crumb flaking also occurred at midpoint of sidewalls. This was analogous to that for all hole-containing specimens.

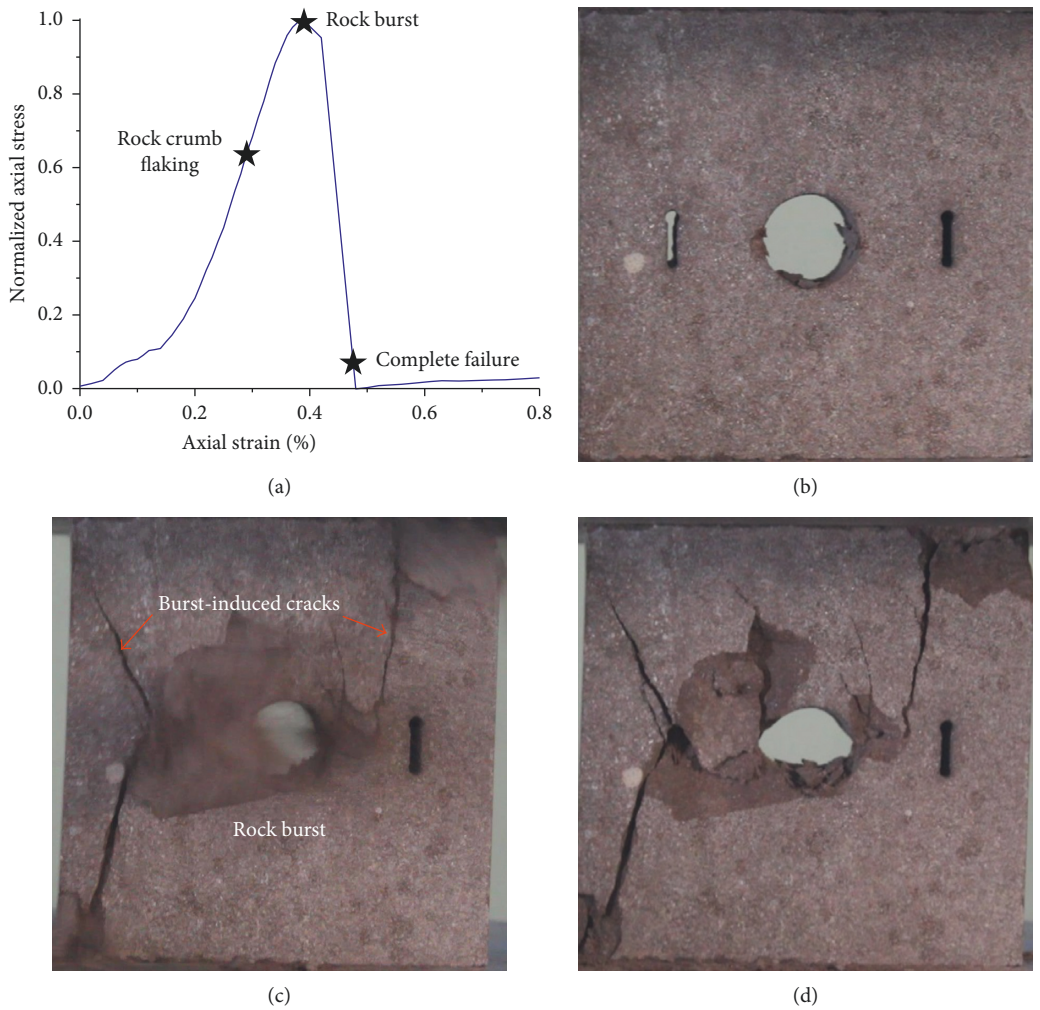

Figure 7: Failure process of the SHTF-90 specimen: (a) stress-strain curve of SHTF-90; (b) rock crumb flaking; (c) rock burst; (d) complete failure.

For the THSF-0 specimen, as seen from the curve in Figure 8(a), when the axial stress was over 60% of peak stress, rock crumb mainly flaked off at internal sidewalls, and then the ligament zones were fast crushed at outer sidewalls at peak stress (Figures 8(b) and 8(c)). Before peak stress, crack never initiated and propagated. The ligament length was 5 mm only, so it crushed easily. The flaw gap became narrow which indicated that the upper block fell down when ligament rock was crushed as shown in Figure 8(d). In the case of the THSF-0 specimen, no rock burst occurred. Obviously, one fragment ejected out at the falling phase of the stress-strain curve.

For the THSF-60 specimen, as usual, as presented on the stress-strain curve in Figure 9(a), rock crumb was first observed at sidewalls (Figure 9(b)). Next, cracks initiated at midpoint of internal sidewalls and then were trying to propagate towards adjacent flaw tip before peak stress. Due to stress concentration at ligament zones, slight rock burst occurred between two holes relative to the burst phenomenon observed in SHTF specimens. Rock burst resulted in crack coalescence as seen in Figure 9(c). Once crack connected the flaw tip to sidewall, the specimen was completely destructive. At the moment of crack coalescence, upper rock block declined, so a shear crack was generated in the upper left specimen. Upper block squeezed left block in the falling process, which resulted in a tensile crack located in left-lower corner (can be seen in Figures 9(c) and 9(d)). As loading continued after peak stress, the ligament zones connecting two holes were crushed and another tensile crack was generated in the upper right corner. Compared with failure process of the Series IV specimen, obviously, the midflaw inclination angle significantly influenced failure behaviors of THSF specimens. Because the ligament was quite short, it was easily crushed. Ligament crush may result in slight increase in axial stress in the residual stage.

For the THSF-90 specimen, rock crumb flaked off at hole side edge, at the stress level like THSF-60 (Figure 10(a)), which can be observed on the opposite side of viewing face as shown in Figure 10(b). Before peak axial stress, no crack initiated around 90° flaw. Actually, crack was hardly generated around 90° flaw, as shown by SHTF-90 in Figure 7. As analyzed in the failure process of the THWF specimen, internal stress intensively distributed within the area between two holes. As illustrated in Figure 10(b), rock block

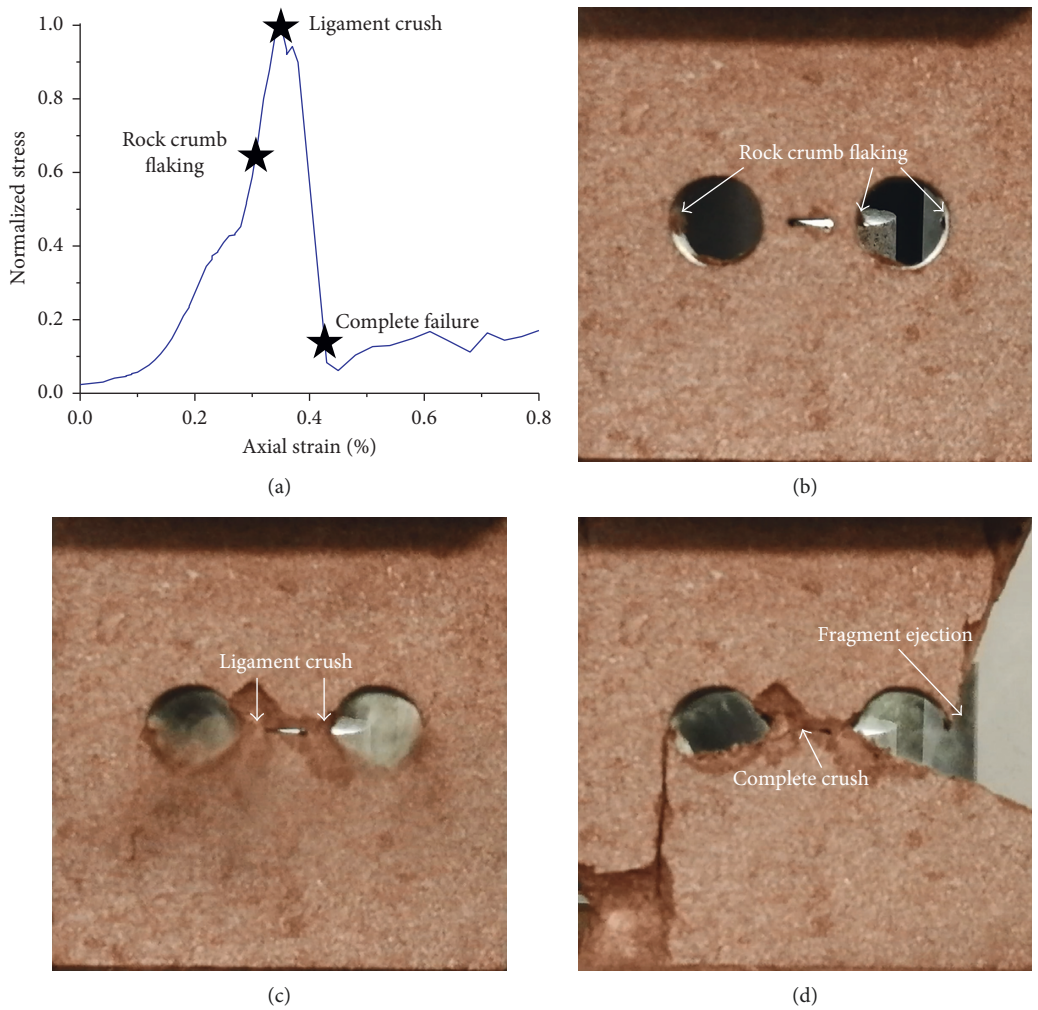

Figure 8: Final failure of the THSF-0 specimen: (a) stress-strain curve of THSF-0; (b) rock crumb flaking; (c) ligament crush; (d) complete failure.

located at both sides of 90° flaw, which can be regarded as rock pillars, subjected to internal concentrated stress. Therefore, the surface rock fragment at the stress-concentrated zone ejected out at failure moment companying with new crack generation at the peak stress level, and then the first crater was generated as shown in Figure 10(c). As loading continued, rock block on top of holes fell, which resulted in right-upper tensile crack. And extrusion between upper and lower blocks brought about surface fragment spalling (Figure 10(d)). Consequently, a second crater was formed as shown in Figure 10(e). The second crater was much bigger than the first one.

For THSF-30 and -60 specimens, an obvious cracking process was observed, but for THSF-90, no crack was generated around 90° flaw, but a crater was created. Basically, due to unequal fall of the upper block, a tensile crack at the upper right corner was generated for 30°, 60°, and 90° specimens. For 0°, 30°, and 60° specimens, a shear crack was generated at the left upper block, and a tensile crack was generated in right lower because of extrusion. Eventually, circles became small after specimen failure due to axial compression.

4. Discussions

Open flaws and circular holes within rock specimens can be considered as defects. Existence of these defects may change internal stress distribution within rock specimens under loading. In this study, flaw location, flaw number, and inclination angle were changed to investigate the effect of these factors on cracking process. Some differences and similarities can be identified in the failure process of various flawed specimens. According to the analysis of the failure process of all specimens, the following four typical failure stages were summarized.

4.1. First Failure Stage: Rock Crumb Flaking. Rock crumb flaking was firstly observed in the whole failure process of all holey specimens, Rock crumb flaking was firstly observed in the whole failure process of all holey specimens. It merely occurred at midpoint of sidewalls of both single-hole and two-hole specimens, but did not occur at top edge or bottom edge of open holes, and even around open flaw. This failure phenomenon was regarded as the first failure stage. Outlet

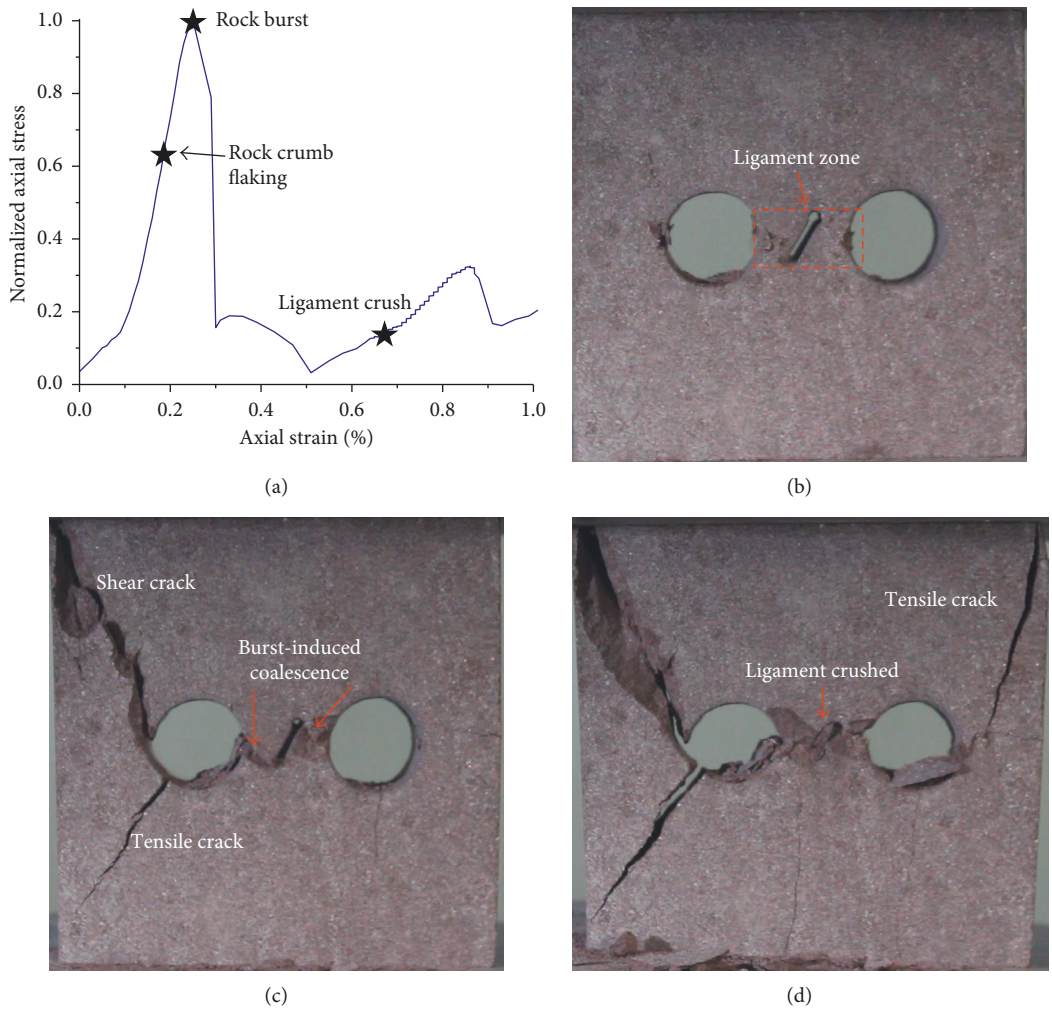

Figure 9: Failure process of the THSF-60 specimen: (a) stress-strain curve of THSF-60; (b) rock crumb flaking; (c) rock burst; (d) ligament crush.

stress concentration in elasticity theory can be used to account for rock crumb flaking that occurred at certain location. Under uniaxial compression, the maximum internal stress concentrated at sidewalls. So the zone that maximum stress located was coincided with the site where rock crumb flaked off. As a matter of fact, in rock tunnel engineering under high geostress, rock fragments still flaked off from inwalls, which is often regarded as a precursor of rock burst. Note that rock crumb flaking mentioned in the present study was observed under uniaxial compressive loading.

4.2. Second Failure Stage: Crack Initiation and Propagation. No matter whether flaws were existed or not, in the early loading phase, rock crumb flaked off at internal stress concentrated locations, which indicated that the flaw arranged outside of open hole hardly changed maximum stress location. Actually, failure around open hole was also associated with the height-to-length ratio, diameter-to-length ratio, and specimen width. When flaw was located within the stress concentrated zone, during loading, stress concentration also occurred at flaw tips, which was indicated by crack initiation at flaw tip. But obviously, crack initiation around open flaw was later than rock crumb flaking around circular hole. When two flaws were located on both sides of hole, tensile crack initiating at flaw tip can be observed except the SHTF-90 specimen. For the SHTF-60 specimen, crack firstly initiated at flaw tip, then propagated towards hole side edge, and finally coalesced on surface. Basically, no crack initiated around open hole. In addition, at the moment that the specimen completely failed, that is, rock burst, several cracks were generated, such as SHTF-30, -60, and -90. Moreover, due to extrusion between rock fragments, new shear or tensile cracks were generated, which mainly occurred after peak strength, such as THSF-0, -30, and -60 specimens.

4.3. Third Failure Stage: Rock Burst. Excavation in natural rock masses under high geostress may result in rock burst, Excavation in natural rock masses under high geostress may result in rock burst. Rock fragments often eject out. As described previously, rock burst was basically observed in all specimens except intact block, SHTF-0 and THSF-0 specimens. Rock burst mainly occurred at the stress-concentrated zone because arrangements of flaw and hole were various for all hole-existent specimens, and the maximum internal

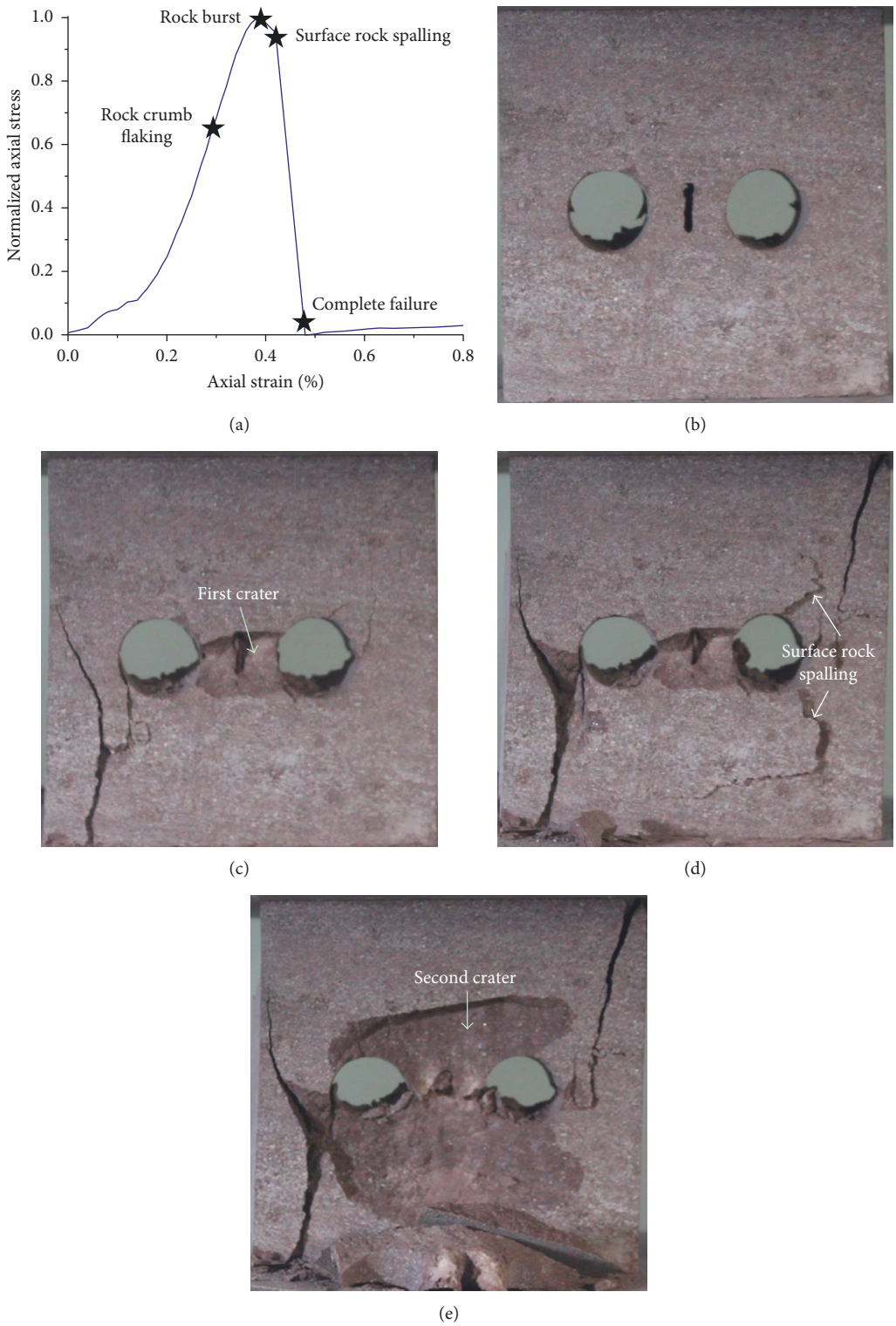

Figure 10: Failure process of the THSF-90 specimen: (a) stress-strain curve of THSF-90; (b) rock crumb flaking; (c) burst-induced crater; (d) surface rock spalling; (e) complete failure.

stress for each series of specimens was various. So the intensive degree of burst was various. Generally, rock burst occurred around open hole, and rock blasted more intensively for single-hole-existent-only specimens. For instance, rock fragments ejected out as shown in Figure 3.

4.4. Fourth Failure Stage: Second Rupture. The axial stress of most tested specimens reached peak strength at the moment of rock burst, but after peak strength, the ligament zone of some specimens was still able to bear loading to some degree as loading continued. In this situation, rock within the

ligament zone may be further crushed which was called second rupture. Rock burst and burst-induced crack was regarded as first rupture. Obviously, as shown in the failure figures, second rupture just was observed in several specimens, which mainly occurred in the tests of SHTF-60 and THSF specimens, especially for SHTF-60 and THSF-90 as shown in Figures 5(e) and 10(e), respectively. Sometimes, rock burst created a small crater and second rupture created a bigger one. For THSF-0, -30, and -60 specimens, ligament rock was crushed in second rupture. Second rupture may slightly increase axial stress after peak strength because of resistance from ligament rock. Second rupture was observed only in case that continuous loading was applied after first rupture.

The experienced failure stages for all hole-and-flaw-containing specimens were summarized. As shown in Table 2, the first stage was essential for all hole-existent specimens regardless of existence of flaw and flaw location arranged in the present study. The second failure stage was mainly observed for the flaw inclination angle of 0° or 30° in the case of SHTF specimens. Additionally, in the loading process of THSF-30, -60, and SHTF-60 specimens, it also can be observed. Note that it did not occur when the flaw inclination angle was 90°. The third failure stage was commonly observed which disabled holey specimens. The fourth failure stage only occurred in a few specimens. In addition, surface rock spalling phenomenon was observed in most specimens during loading. It mainly occurred at stress concentration zones, inducing by rock burst or extrusion between rock blocks.

High-compressive stress concentrates at hole side edges, and tensile stress may concentrate at top and bottom edges. Stress magnitude is directly related to the applied external loading. Concentrated tensile stress is much smaller than concentrated compressive stress around hole. As stated above, different combinations of hole and flaw may experience various failure stages. For SHWF and THWF specimens, rupture merely occurred at sidewalls, and the two cases experienced failure at Stage I and II only, that is, rock crumb flaking and rock burst. On the basis of hole-containing-only specimens, premanufactured flaw may disturb internal stress distribution which may be different from that of SHWF and THWF specimens under external loading. Stress distribution depended on flaw arrangement. In the case of THSF specimens, failure at sidewalls of two holes is similar to that of single-hole case. Failure around midflaw is related to the flaw inclination angle and ligament.

For brittle materials, according to Griffith [50], stress concentrates at flaw tip. When strain energy accumulates to some degree, which exceeds tensile strength of brittle material, crack initiates at flaw tip and then propagates along the direction perpendicular to maximum tensile stress at tip. It well explains that crack often initiates at flaw tip as observed in Figures 4 and 5. Open hole greatly changes internal stress distribution relative to intact specimen, top flaw is located at nonstress concentration area, and during compressive loading, top flaw scarcely forms stress concentration at flaw tip. For SHTF specimens, two open flaws were located at stress concentration area, flaw resulted in stress redistribution relative to the SHTF specimen, and flaw tip formed stress concentration, so visible cracks were generated at flaw tips during loading. For THSF specimens, middle flaw was also located in the stress concentration area of two holes. Flaw also formed stress concentration at tips, so cracks initiated and propagated for THSF-30 and -60. Due to short ligament between inner edge and flaw tip for THSF-0, ligament was directly crushed, so no crack initiated. When $\alpha = 90°$, crack never initiated due to the small angle between flaw inclination angle and maximum principal stress at flaw tip. So among the tested cases, flaw located in stress concentration dramatically influenced failure process, especially failure Stage II.

Table 2: Category of experienced failure stages.

		Stage I	Stage II	Stage III	Stage IV
SHTF	0	★	★	☆	☆
	30	★	★	★	☆
	60	★	★	★	★
	90	★	☆	★	☆
THSF	0	★	☆	☆	★
	30	★	★	★	★
	60	★	★	★	★
	90	★	☆	★	★

Note. ★ = experienced; ☆ = Non-experienced.

As known, friction effect exists on the interface between the platen and sample end. It affects the stress distribution in sample under compressive loading. Generally, painting lubricant or adding plastic plate between the sample end and platen is used to decrease friction effect. If the stiffness of the added plate is smaller than that of the rock sample, tensile stress may be induced. Certainly, complete avoiding end effect is quite hard except that the platen stiffness is equal to rock sample stiffness. In the current test, lubricant was used to decrease friction effect, and the painted lubricant is thin. Furthermore, the sample ends are smoothly machined. In the duration of whole loading, no tensile failure phenomenon was observed around sample ends. So it can be regarded as that tensile stress hardly occurs at sample ends. Even though tensile stress was induced close to the sample end, it was small and could not destruct the sample.

5. Conclusions

In a sandstone specimen, open flaws and cylindrical holes were created using high-pressure water jet cutting technology. Through changing the relative location and number of flaws and holes, various flawed specimens were made. Uniaxial compressive tests were performed to investigate the failure process of flawed and holey specimens. The following conclusions can be established from the presented results in this study:

(1) For hole-existent specimens without flaw, rock crumb flaking was firstly occurred at sidewalls, and its failure was blast-induced and usually created crater at stress-concentrated zone. Under uniaxial compression, open hole remarkably disturbed internal stress distribution, especially at sidewalls of hole, which resulted in rock crumb flaking.

(2) Rock burst was the major failure mode and generally observed but not in the intact block, SHTF-0 and THTF-0 specimens. Occurrence of rock burst, which

usually companied with huge sonic, generated crater around open hole and made rock fragment eject out.

(3) In the series of SHTF specimens under uniaxial compression, rock crumb flaking was firstly observed in the process of loading. For SHTF-0 and -30 specimens, tensile cracks initiated at flaw tips, which was not observed for SHTF-60 and -90 specimens. Rock burst occurred except for the SHTF-0 specimen, which generated crater for SHTF-60 and -90 specimens. Some new shear or tensile cracks were induced by rock burst or rock fragment extrusion.

(4) In the case of THSF specimens under uniaxial compression, stress concentration mainly occurred between two open holes, and secondarily at outer sidewalls. Rock crumb flaking was firstly observed at internal sidewalls and then outer sidewalls. For the THSF-0 specimen, ligament zones between internal sidewall and adjacent flaw tip were easily crushed. For THSF-30 and -60 specimens, crack initiated at internal sidewall and propagated and finally connected sidewall and adjacent flaw tip, which did not occur for the 90° specimen. For THSF-90 specimens, slight rock burst occurred at the ligament zone and generated a small crater, but eventually a big crater was created due to extrusion between upper and lower blocks after first crater generation. Some tensile and shear cracks were generated for THSF specimens during upper block decline.

Conflicts of Interest

The authors declare that there are no conflicts of interest regarding the publication of this paper.

Acknowledgments

This research was financially supported by the Fundamental Research Funds for the Central Universities (310821161008), China Postdoctoral Science Foundation (2016M602742), National Natural Science Foundation of China (51774322 and 51474249), Open Fund of State Key Laboratory of Geohazard Prevention and Geoenvironment Protection (SKLGP2016K009), the Traffic Construction Research Funds of Shanxi Province (2017-1-4), Open Fund of Key Laboratory of Bridge Engineering Safety Control by Hunan Province, Department of Education (Changsha University of Science and Technology) (15KB02), and Open Fund of Engineering Research Center of Catastrophic Prophylaxis and Treatment of Road & Traffic Safety of Ministry of Education (Changsha University of Science and Technology) (kfj150405).

References

[1] E. Hoek and Z. T. Bieniawski, "Brittle fracture propagation in rock under compression," *International Journal of Fracture Mechanics*, vol. 1, no. 3, pp. 137–155, 1965.

[2] E. Z. Lajtai, "Brittle fracture in compression," *International Journal of Fracture*, vol. 10, no. 4, pp. 525–536, 1974.

[3] A. Bobet and H. H. Einstein, "Numerical modeling of fracture coalescence in a model rock material," *International Journal of Fracture*, vol. 92, no. 3, pp. 221–252, 1998.

[4] L. N. Y. Wong and H. H. Einstein, "Crack coalescence in molded gypsum and Carrara marble: part 1. Macroscopic observations and interpretation," *Rock Mechanics and Rock Engineering*, vol. 42, no. 3, pp. 475–511, 2009.

[5] Y. F. Yang, C. A. Tang, and K. W. Xia, "Study on crack curving and branching mechanism in quasi-brittle materials under dynamic biaxial loading," *International journal of fracture*, vol. 177, no. 1, pp. 53–72, 2012.

[6] X. P. Zhang and L. N. Y. Wong, "Cracking processes in rock-like material containing a single flaw under uniaxial compression: a numerical study based on parallel bonded-particle model approach," *Rock Mechanics and Rock Engineering*, vol. 45, no. 5, pp. 711–737, 2012.

[7] M. Bahaaddini, G. Sharrock, and B. K. Hebblewhite, "Numerical investigation of the effect of joint geometrical parameters on the mechanical properties of a non-persistent jointed rock mass under uniaxial compression," *Computers and Geotechnics*, vol. 49, no. 4, pp. 206–225, 2013.

[8] P. H. S. W. Kulatilake, W. He, J. Um, and H. Wang, "A physical model study of jointed rock mass strength under uniaxial compressive loading," *International Journal of Rock Mechanics and Mining Sciences*, vol. 34, no. 3, pp. 165.e1–165.e15, 1997.

[9] A. Bobet and H. H. Einstein, "Fracture coalescence in rock-type materials under uniaxial and biaxial compression," *International Journal of Rock Mechanics and Mining Sciences*, vol. 35, no. 7, pp. 863–888, 1998.

[10] Y. L. Zhao, L. Zhang, W. Wang, C. Pu, W. Wan, and J. Tang, "Cracking and stress–strain behavior of rock-like material containing two flaws under uniaxial compression," *Rock Mechanics and Rock Engineering*, vol. 49, no. 7, pp. 2665–2687, 2016.

[11] T. Liu, B. Lin, W. Yang, Q. Zou, J. Kong, and F. Yan, "Cracking process and stress field evolution in specimen containing combined flaw under uniaxial compression," *Rock Mechanics and Rock Engineering*, vol. 49, no. 8, pp. 3095–3113, 2016.

[12] S. Q. Yang and H. W. Jing, "Strength failure and crack coalescence behavior of brittle sandstone samples containing a single fissure under uniaxial compression," *International Journal of Fracture*, vol. 168, no. 2, pp. 227–250, 2011.

[13] X. Chen, Z. Liao, and X. Peng, "Deformability characteristics of jointed rock masses under uniaxial compression," *International Journal of Mining Science and Technology*, vol. 22, no. 2, pp. 213–221, 2012.

[14] X. Chen, Z. H. Liao, and X. Peng, "Cracking process of rock mass models under uniaxial compression," *Journal of Central South University*, vol. 20, no. 6, pp. 1661–1678, 2013.

[15] X. P. Zhang, L. N. Y. Wong, and S. Wang, "Effects of the ratio of flaw size to specimen size on cracking behavior," *Bulletin of Engineering Geology and the Environment*, vol. 74, no. 1, pp. 181–193, 2015.

[16] L. D. Suits, T. C. Sheahan, L. N. Y. Wong, and H. H. Einstein, "Using high speed video imaging in the study of cracking processes in rock," *Geotechnical Testing Journal*, vol. 32, no. 2, pp. 1–17, 2009.

[17] C. A. Tang and S. Q. Kou, "Crack propagation and coalescence in brittle materials under compression," *Engineering Fracture Mechanics*, vol. 61, no. 3, pp. 311–324, 1998.

[18] R. H. Wong and K. T. Chau, "Crack coalescence in a rock-like material containing two cracks," *International Journal of Rock Mechanics and Mining Sciences*, vol. 35, no. 2, pp. 147–164, 1998.

[19] R. H. C. Wong, K. T. Chau, C. A. Tang, and P. Lin, "Analysis of crack coalescence in rock-like materials containing three flaws—part I: experimental approach," *International Journal of Rock Mechanics and Mining Sciences*, vol. 38, no. 7, pp. 909–924, 2001.

[20] R. H. C. Wong, P. Lin, C. A. Tang, and K. T. Chau, "Creeping damage around an opening in rock-like material containing non-persistent joints," *Engineering fracture mechanics*, vol. 69, no. 17, pp. 2015–2027, 2002.

[21] A. Bobet, "The initiation of secondary cracks in compression," *Engineering Fracture Mechanics*, vol. 66, no. 2, pp. 187–219, 2000.

[22] C. H. Park and A. Bobet, "Crack coalescence in specimens with open and closed flaws: a comparison," *International Journal of Rock Mechanics and Mining Sciences*, vol. 46, no. 5, pp. 819–829, 2009.

[23] S. Q. Yang, H. W. Jing, and S. Y. Wang, "Experimental investigation on the strength, deformability, failure behavior and acoustic emission locations of red sandstone under triaxial compression," *Rock mechanics and rock engineering*, vol. 45, no. 4, pp. 583–606, 2012.

[24] H. Lee and S. Jeon, "An experimental and numerical study of fracture coalescence in pre-cracked specimens under uniaxial compression," *International Journal of Solids and Structures*, vol. 48, no. 6, pp. 979–999, 2011.

[25] H. Lin, X. Wei, and Q. X. Yan, "Three-dimensional effect of tensile strength in the standard Brazilian test considering contact length," *Geotechnical Testing Journal*, vol. 39, no. 1, p. 20140268, 2016.

[26] Y. H. Huang, S. Q. Yang, W. L. Tian, W. Zeng, and L. Y. Yu, "An experimental study on fracture mechanical behavior of rock-like materials containing two unparallel fissures under uniaxial compression," *Acta Mechanica Sinica*, vol. 32, no. 3, pp. 442–455, 2015.

[27] Y. Zhao, L. Zhang, W. Wang, J. Tang, H. Lin, and W. Wan, "Transient pulse test and morphological analysis of single rock fractures," *International Journal of Rock Mechanics & Mining Sciences*, vol. 91, pp. 139–154, 2017.

[28] M. Prudencio and M. V. S. Jan, "Strength and failure modes of rock mass models with non-persistent joints," *International Journal of Rock Mechanics and Mining Sciences*, vol. 44, no. 6, pp. 890–902, 2007.

[29] M. Adams and G. Sines, "Crack extension from flaws in a brittle material subjected to compression," *Tectonophysics*, vol. 49, no. 1, pp. 97–118, 1978.

[30] L. N. Germanovich, R. L. Salganik, A. V. Dyskin, and K. K. Lee, "Mechanisms of brittle fracture of rock with pre-existing cracks in compression," *Pure and Applied Geophysics*, vol. 143, no. 1–3, pp. 117–149, 1994.

[31] A. V. Dyskin, L. N. Germanovich, and K. B. Ustinov, "A 3-D model of wing crack growth and interaction," *Engineering Fracture Mechanics*, vol. 63, no. 1, pp. 81–110, 1999.

[32] N. C. Gay, "Fracture growth around openings in large blocks of rock subjected to uniaxial and biaxial compression," *International Journal of Rock Mechanics and Mining Sciences & Geomechanics Abstracts*, vol. 13, no. 12, pp. 231–243, 1976.

[33] R. T. Ewy and N. G. W. Cook, "Deformation and fracture around cylindrical openings in rock—I. Observations and analysis of deformations," *International Journal of Rock Mechanics and Mining Sciences & Geomechanics Abstracts*, vol. 27, no. 5, pp. 387–407, 1990.

[34] R. T. Ewy and N. G. W. Cook, "Deformation and fracture around cylindrical openings in rock—II. Initiation, growth and interaction of fractures," *International Journal of Rock Mechanics and Mining Sciences & Geomechanics Abstracts*, vol. 27, no. 5, pp. 409–427, 1990.

[35] B. J. Carter, E. Z. Lajtai, and Y. Yuan, "Tensile fracture from circular cavities loaded in compression," *International journal of fracture*, vol. 57, no. 3, pp. 221–236, 1992.

[36] A. Golshani, M. Oda, Y. Okui, T. Takemura, and E. Munkhtogoo, "Numerical simulation of the excavation damaged zone around an opening in brittle rock," *International Journal of Rock Mechanics and Mining Sciences*, vol. 44, no. 6, pp. 835–845, 2007.

[37] W. C. Zhu and O. T. Bruhns, "Simulating excavation damaged zone around a circular opening under hydromechanical conditions," *International Journal of Rock Mechanics and Mining Sciences*, vol. 45, no. 5, pp. 815–830, 2008.

[38] C. Zhao, H. Matsuda, C. Morita, and M. R. Shen, "Study on failure characteristic of rock-like materials with an open-hole under uniaxial compression," *Strain*, vol. 47, no. 5, pp. 405–413, 2011.

[39] S. Ma, J. Guo, L. Li, Y. Xia, and T. Yang, "Experimental and numerical study on fracture propagation near open-hole horizontal well under hydraulic pressure," *European Journal of Environmental and Civil Engineering*, vol. 20, no. 4, pp. 412–430, 2016.

[40] X. D. Zhao, H. X. Zhang, and W. C. Zhu, "Fracture evolution around pre-existing cylindrical cavities in brittle rocks under uniaxial compression," *Transactions of Nonferrous Metals Society of China*, vol. 24, no. 3, pp. 806–815, 2014.

[41] Y. Li, J. Peng, F. Zhang, and Z. Qiu, "Cracking behavior and mechanism of sandstone containing a pre-cut hole under combined static and dynamic loading," *Engineering Geology*, vol. 213, no. 11, pp. 64–73, 2016.

[42] C. D. Martin, R. S. Read, and J. B. Martino, "Observations of brittle failure around a circular test tunnel," *International Journal of Rock Mechanics and Mining Sciences*, vol. 34, no. 7, pp. 1065–1073, 1997.

[43] J. B. Martino and N. A. Chandler, "Excavation-induced damage studies at the underground research laboratory," *International Journal of Rock Mechanics and Mining Sciences*, vol. 41, no. 8, pp. 1413–1426, 2004.

[44] X. P. Zhang and L. N. Y. Wong, "Crack initiation, propagation and coalescence in rock-like material containing two flaws: a numerical study based on bonded-particle model approach," *Rock mechanics and rock engineering*, vol. 46, no. 5, pp. 1001–1021, 2013.

[45] X. Fan, P. H. S. W. Kulatilake, and X. Chen, "Mechanical behavior of rock-like jointed blocks with multi-non-persistent joints under uniaxial loading: a particle mechanics approach," *Engineering Geology*, vol. 190, no. 5, pp. 17–32, 2015.

[46] M. Sagong, D. Park, J. Yoo, and J. S. Lee, "Experimental and numerical analyses of an opening in a jointed rock mass under biaxial compression," *International Journal of Rock Mechanics and Mining Sciences*, vol. 48, no. 7, pp. 1055–1067, 2011.

[47] X. Yang, H. Jing, and K. Chen, "Numerical simulations of failure behavior around a circular opening in a non-persistently jointed rock mass under biaxial compression," *International Journal of Mining Science and Technology*, vol. 26, no. 4, pp. 729–738, 2016.

[48] P. Jia and C. A. Tang, "Numerical study on failure mechanism of tunnel in jointed rock mass," *Tunnelling and Underground Space Technology*, vol. 23, no. 5, pp. 500–507, 2008.

[49] W. C. Zhu, J. S. Liu, C. A. Tang, X. D. Zhao, and B. H. Brady, "Simulation of progressive fracturing processes around underground excavations under biaxial compression," *Tunnelling and Underground Space Technology*, vol. 20, no. 3, pp. 231–247, 2005.

[50] A. A. Griffith, "The phenomena of rupture and flow in solids. Philosophical Transactions of the Royal Society of London," *Series A, Containing Papers of a Mathematical or Physical Character*, vol. 221, pp. 163–198, 1921.